JOURNAL OF SOLID STATE CHEMISTRY 61, 67–80 (1986)

X-Ray Induced Defects and Thermoluminescent Properties of Lanthanum Hexaaluminates with Magnetoplumbite-like Structure

D. GOURIER, F. LAVILLE, AND D. VIVIEN

Laboratoire de Chimie Appliquée de l'État Solide, LA 302 CNRS, 11 Rue Pierre et Marie Curie 75231 Paris Cédex 05, France

AND C. VALLADAS

Centre des Faibles Radioactivités, Domaine du CNRS, Avenue de la Terrasse 91190 Gif sur Yvette, France

Received March 25, 1985; in revised form June 10, 1985

This work presents an electron spin resonance and optical study of the defects produced by X-ray irradiation of the lanthanum aluminate $La(Mg_{1-y}Mn_y)_xAl_{11}O_{18+x}$ ($x, y \leq 1$). The thermal bleaching of these defects is responsible for an intense green thermoluminescence due to the $^4T_1$–$^6A_1$ transition of Mn^{2+} ions of the lattice. The mechanism of this thermoluminescence and its variation with manganese concentration are discussed. © 1986 Academic Press, Inc.

I. Introduction

X-Ray irradiation of ionic solids usually modifies the electrical charge distribution inside the material. For instance, in the superionic conductor β-alumina ($Na_xAl_{11}O_{17+x/2}$, $x \simeq 1.3$), exposure to X rays partially converts oxygen vacancies of the conduction planes, into F^+ centers (*1*). Spectroscopic methods such as optical absorption and electron spin resonance (ESR) can consequently be used to study these paramagnetic F^+ centers (*1*), thus giving information about their precursor defects which cannot be investigated by these techniques.

The present paper deals with lanthanide hexaaluminates of the general formula $Ln\,M_xAl_{11}O_{18+x}$ ($x \leq 1$) with magnetoplumbite-like (MP) structure. The hexagonal unit cell (*2–3*)—which is quite similar to that of the β-alumina,—is made of spinel blocks (four oxygen layers) containing Al^{3+} and/or M^{2+} ions in octahedral or tetrahedral sites separated by mirror planes containing Ln^{3+}, three oxygen ions, and Al^{3+} in four- or five-fold coordination (*3*) (Fig. 1). Actually, the O^{2-} coordination polyhedra of the aluminum site is a trigonal bipyramid with the z axis along the **c** crystal direction, but Al^{3+}, which no longer lies in the mirror plane, is shifted on the z axis toward one of the two axial oxygen ions (*3*).

These lanthanide hexaaluminates received attention during the past decade because of their very efficient luminescent properties (*4*). Recently we reported the observation of continuous laser effect (*5*) in

0022-4596/86 $3.00

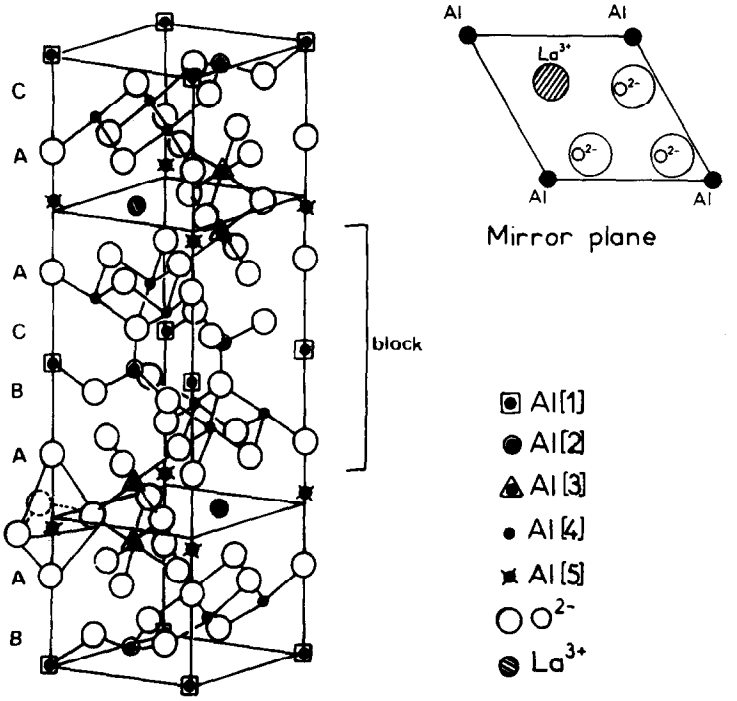

FIG. 1. Magnetoplumbite structure.

Czochralski-grown single crystals of $La_{0.9}Nd_{0.1}MgAl_{11}O_{19}$ (LNA). This effect has also been reported independently by Russian workers (*6*), showing that LNA is a very interesting solid-state laser material which may compete with yttrium–aluminum garnet (YAG:Nd), presently the most commercial important neodymium solid-state laser.

An important point to be considered concerning the potential application of a new material is durability under working conditions. Actually, some β-alumina or MP-like phosphors depreciate under UV irradiation (*7*), and laser action of rare-earth ions in perovskite $YAlO_3$ is hindered by the coloration of the crystal arising from defect centers generated from the action of pump light (8). Colorless MP lanthanum aluminates also turn brownish when submitted to UV, X, or γ radiations. Owing to the properties of these compounds, we have been prompted to study the radiation-induced centers responsible for this coloration in $LaMg_xAl_{11}O_{18+x}$ using both ESR and optical absorption (OA) spectroscopy in the UV-visible range. Thermal recombination of these centers leads to a strong thermally stimulated luminescence (TSL) which proceeds through Mn^{2+} ions present in the lattice as impurity. This led us to study the whole series of compounds $LaM_xAl_{11}O_{18+x}$ ($M = Mg_{1-y}Mn_y$; $x, y \leq 1$) whose structure and crystal growth have already been investigated in our laboratory (*3*, *9*, *10*).

II. Experimental

Single crystals of lanthanum aluminates $LaM_xAl_{11}O_{18+x}$ ($M = Mg_{1-y}Mn_y$, $x, y \leq 1$), referred to as $LA_{x,y}$, were grown by the flame fusion method (Verneuil process) (*9*, *10*). The starting material was an intimate mixture of the constitutive oxides, and the

TABLE I

MANGANESE CONTENT (y) OF THE CRYSTALS $La(Mg_{1-y}Mn_y)_xAl_{11}O_{18+x}$ COMPARED WITH THEIR STARTING (THEORETICAL) COMPOSITIONS (y_{th})

Y_{th}	~0	0.02	0.1	0.25	0.50	0.75	1
y	5 to 10 ppm[a]	0.01	0.07	0.15	0.27	0.40	0.44

[a] The Mn concentration was estimated by comparing the ESR intensity of Mn^{2+} with that of a single crystal of $Na_{1.3}Al_{11}O_{17.65}$ (β-alumina) whose Mn concentration has been determined by atomic absorption spectroscopy.

growth rate about 1 cm · h^{-1} (*9, 10*). Single crystalline platelets, typically 5 × 5 × 1 mm^3 were easily cleaved from the Verneuil boules, along the (00.1) plane.

The divalent content of the crystal was estimated by using a Camebax-Microbeam electron microprobe (*11*). This analysis indicated that the compounds $LA_{x,y}$ suffered a loss of M^{2+} ions during the crystal growth, leading to a significant departure of x and y from their starting values. For instance, the starting compositions $LaMgAl_{11}O_{19}$ ($LA_{1,0}$) and $LaMnAl_{11}O_{19}$ ($LA_{1,1}$) led to crystals with composition $LA_{0.9,0}$ and $LA_{0.44,0.44}$, respectively. Since the loss of Mg is nearly constant (~15%) the crystals studied in the following sections will be identified according to their final Mn composition (y value) as LA_y. The Mn contents in both the starting materials and the single crystals are gathered in Table I.

The UV-visible absorption spectra were recorded at room temperature with a Pye–Unicam SP 1800 spectrometer and in the liquid-helium temperature range with a Beckmann UV 5270 spectrometer fitted with an Oxford Instruments helium flow cryostat. Computer fitting of the spectra to a sum of Gaussian-shaped lines allowed accurate determination of the peak positions and linewidths.

The ESR spectra were run on a Brucker ER 220D spectrometer equipped with a variable temperature accessory (100–300 K). The crystals were mounted on a small Perspex sample holder to allow their orientation with respect to the magnetic field. This was calibrated using a Bruker NMR proton BNM 12 and the microwave frequency was measured with a Systron–Donner frequency counter. Both OA and ESR spectra of the crystals were recorded as soon as it was possible (~5–10 minutes) after irradiation.

Irradiation of samples was performed at room temperature using 40-kV, 20-mA X rays from a copper target tube. The unfiltered X radiations consist mainly of $K\alpha$ (1.54 Å) and $K\beta$ (1.39 Å) emission of copper. TSL experiments were performed after irradiation of the samples by 2-MeV β radiation from a ^{90}Y source. In order to ensure good thermal contact, the crystals were finely ground and only a thin layer of the 100- to 160-μm fraction was deposited in the heated stainless-steel sample holder.

III. Thermally Stimulated Luminescence of LA_y

Single crystals of LA_y exhibit a strong green TSL after irradiation by X rays. This TSL is characterized by the following features.

(i) The light emission is green, over the entire temperature range at which this TSL is detected, e.g., between room temperature and ~300°c.

(ii) The intensity of the green emission is maximum for the compound $La_{0.01}$. LA_0 exhibits a TSL only at $T > 130$°C while a strong emission is detectable at room temperature in LA_y with $y \geq 0.01$. In the latter compounds, the green light is detectable with the naked eye after only a few seconds of exposure to X rays.

(iii) For a fixed time of exposure, the afterglow exhibits only a slight decrease of its intensity with increasing y for $y \geq 0.07$,

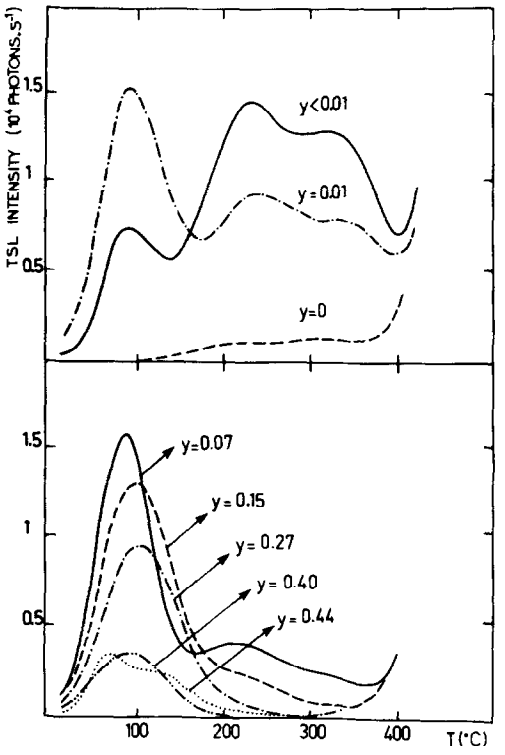

FIG. 2. TSL glow curves of LA_y irradiated at room temperature. β-Ray dose: 75 mrad. The curves are recorded using filters with maximum transmission at 550 nm.

while the intensity of the TSL at higher temperature, e.g., ~300°C, strongly decreases with increasing y, and is no longer detectable for $y > 0.07$. All these features are confirmed and further clarified by investigation of the β radiation-induced TSL. Figure 2 shows the glow curves of compounds LA_y with y varying from $\simeq 0$ ([Mn] $\simeq$ 5–10 ppm) to 0.44. The β ray doses were 75 mrad in each case and the curves were recorded by using a filter with maximum transmission at 550 nm (green). There are three glow peaks at ~95, ~210, and ~320°C, whose intensities depend on the Mn content of the compound. For $y \simeq 0$, the peak at $\simeq$95°C is missing. Increasing y to 0.01 results in a strong increase of all the TSL peaks. For $y > 0.01$ the peak intensities decrease with increasing y, the reduction of the 210 and 320°C peak intensities being more pronounced than the 95°C one. These features indicate that the green TSL is due to the $^4T_1 \rightarrow {}^6A_1$ transition of Mn^{2+} ions. Previous studies of LA_y have shown that Mn^{2+} ions are localized in tetrahedral sites of the structure (*10*) and that these ions emit a green photoluminescence at 520 nm (*4*).

The TSL glow curves of the compound LA_0 are shown in Fig. 3. They were recorded using filters with maximum transmission at 550, 500, 425, and 380 nm. The β doses were 500 mrad except for the curve at 380 nm, which was obtained with a dose of 5 rad. The maximum emission is also in the green region, like the Mn-enriched compounds, but a weak violet emission seems to occur at low temperatures.

We have not attempted to make accurate measurements of the activation energy corresponding to each TSL peak. A rough estimate can be obtained from the empirical expression given by Urbach (*12*):

$$E\ (\text{eV}) = T_m/500, \qquad (1)$$

where T_m is the temperature of the glow maximum (in K). Applying (1) to the glow peaks at 95, 210, and 320°C gives activation energies of ~0.7, ~1.0, and ~1.2 eV, respectively. These values correspond to the trap depth energies of the defects responsible for the different TSL peaks. We have

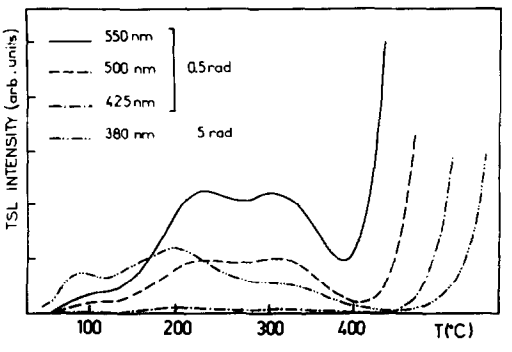

FIG. 3. TSL glow curves of LA_0 recorded with filters in the range 550 nm (green) to 380 nm (violet).

checked the validity of these results by measuring the activation energy E of the 320°C glow peak according to the more accurate method derived by Hoogenstratten (*13*). This method is based on the variation of T_m with the linear heating rates β of the samples. β and T_m are related to the activation energy E by (*13*)

$$\frac{\beta E}{kT_m^2} = s_0 \exp\left(-\frac{E}{kT_m}\right) \qquad (2)$$

where s_0 is the preexponential factor. Plotting $\ln(T_m^2/\beta)$ versus $1/T_m$ using β values in the range 0.6 to 9.1 K sec^{-1} gives $E = 1.38$ eV and $s_0 = 2.15 \times 10^{11}$ sec^{-1}. The agreement with the value $E \simeq 1.2$ eV obtained from expression (1) is fair considering the roughness of the Urbach method.

Lebedev *et al.* (*14*) reported slightly different results for the X-ray-induced TSL of LA_0. These authors have found two glow peaks at 95 and 230°C, the former being much more intense than the latter. The activation energies measured by the initial rise method were 0.69 and 1.37 eV, respectively, and three emission maxima at 350, 520, and 700 nm were found for each glow peak, but the relative intensities of these bands were not specified. Lebedev *et al.* (*14*) ascribed the 700-nm band to Cr^{3+} emission but they failed to interpret the other bands at 520 and 350 nm. It is evident from our experiments on Verneuil-grown crystals of LA_y that the TSL is predominantly due to Mn^{2+} emission. The differences between our results and those of Lebedev *et al.* (*14*) could originate from differences in the sample preparation, their crystals being grown by slow cooling of melts prepared by high frequency heating in cold containers (*14*).

IV. Identification of X-Ray-Induced Defects in LA_0

Optical absorption and Electron Spin Resonance spectroscopies have been used for the identification of defects created by X rays. Our investigations were almost restricted to the compound LA_0 because the manganese ions in LA_y compounds were responsible for two unwanted effects which preclude detailed spectroscopic studies:

(i) The ESR spectra of defects are hidden by the more intense spectrum of Mn^{2+} ions in LA_y for $y > 0.01$.

(ii) The very intense TSL peak at 95°C in LA_y ($y \geq 0.01$) is responsible for an afterglow which interferes with the OA spectrum. Nevertheless, the $LA_{0.01}$ defect spectra appear identical to the LA_0 ones.

IV.1. Radiation-Induced Color Centers

After exposure of LA_0 to X rays one observes in its OA spectrum the appearance of a broad and intense band centered at 3.1 eV (Fig. 4), together with an ESR signal at $g \simeq 2.0$ (Fig. 5). These two signals reach their maximum intensity after an irradiation time of about 60 min. In fact, they grow simultaneously and a linear relation exists between their intensities as shown in Fig. 6. As a consequence these ESR and OA spectra are related to a same defect center which is hereafter labeled A. A simultaneous decrease of both OA and ESR intensities of center A is observed after 5 min thermal annealing at temperatures ranging between room temperature and 180°C. Annealing treatments at temperatures higher than 180°C result in a complete bleaching of the ESR signal while a weak and very broad absorption band peaking near 2.8 eV remains in the OA spectra (Fig. 4). The residual absorption is composed of several bands whose relative intensities depend upon sample preparation and annealing. This indicates that they correspond to several different defects. Recording these OA spectra at low temperature (15 K) improves the resolution and allows the observation of three bands with maxima at 3.8, 2.8, and 2.1 eV, related to three different defects hereafter labeled B, C, and D, respectively.

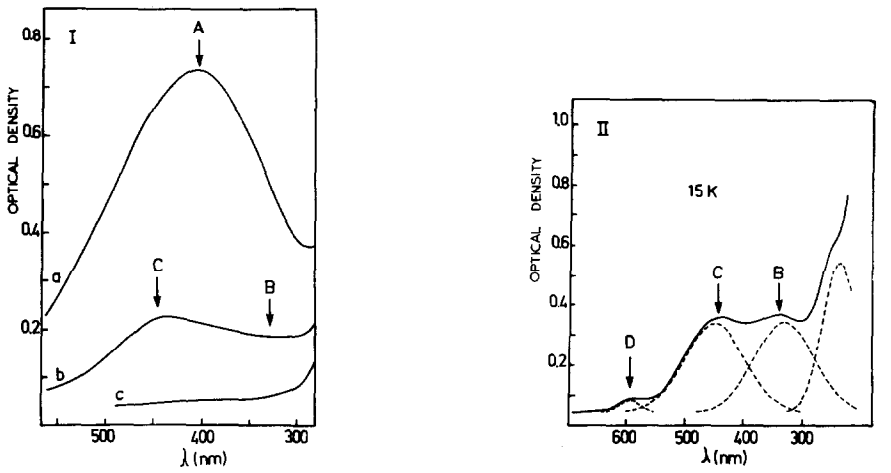

FIG. 4. Optical absorption spectra of LA_0 recorded after 1 hr exposure to X rays. The arrows indicate the absorption bands of defects A, B, C, and D. (I) Room temperature: (a) immediately after irradiation, (b) 5 min at 180°C after irradiation, (c) 15 min at 380°C after irradiation; (II) T = 15 K: 5 min at 180°C after irradiation.

Their intensities decrease upon increase of annealing temperatures above 240°C; complete bleaching of these bands is achieved at 380°C.

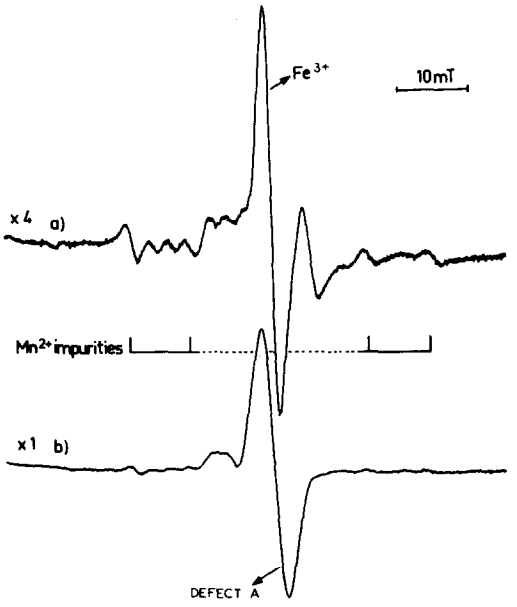

FIG. 5. ESR spectra at 25°C of LA_0 recorded with B_0 parallel to the [00.1] crystallographic axis: (a) nonirradiated; (b) irradiated by X rays for 1 hr.

(*a*). *Identification of defect A.* Figure 5 shows the ESR spectrum of center A in a single crystal of LA_0 irradiated for 1 hr. For an orientation of the static magnetic field B_0 parallel to the [00.1] crystallographic axis (c-axis) the ESR signal of center A is superimposed upon the signal of Fe^{3+} impurities. However, these signals can be separated and studied for a small deviation of B_0 from

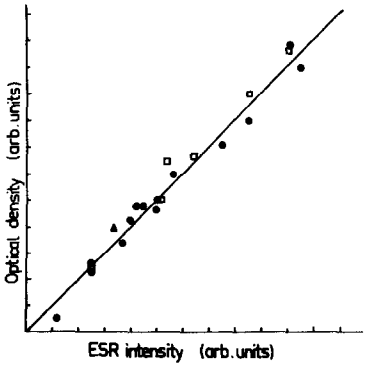

FIG. 6. Linear relationship between the optical density at 3.1 eV and the ESR intensity of defect A in LA_0. Circles, Sample 1; squares, Sample 2. The experimental points were obtained by varying the irradiation time between 1 min and 1 hr. Triangle, sample 1 irradiated for 1 hr and annealed at 130°C for 5 min.

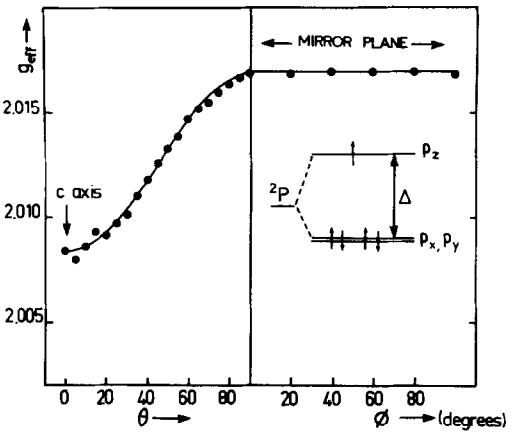

FIG. 7. ESR of defect A in LA_0. Variation of g_{eff} with the orientation of the magnetic field B_0. θ is the deviation from the [00.1] axis and ϕ represents the rotation of B_0 in the mirror plane. The diagram shows the removal of the $O^- - {}^2P$ ground state degeneracy by an adjacent cation vacancy along the z axis.

the [00.1] axis because the g factor anisotropy is much more important for Fe^{3+} than for center A.

The angular variation of the effective g factor g_{eff} of center A can be fitted using an axial g tensor with z colinear to the [00.1] direction and with principal values $g_\parallel = 2.0083$ and $g_\perp = 2.0170$ (Fig. 7). The lineshape is Gaussian, and the linewidth ΔB, which is 3.5 mT for both $B_0 \| [00.1]$ and $B_0 \perp [00.1]$, reaches its maximum value of 4.1 mT for B_0 at 45° from the [00.1] axis. These values of g and ΔB closely resemble those found in γ-ray-induced defects in α-Al_2O_3 (*15*). It is now recognized that these defects are O^- ions ($\equiv O_O^\cdot$ in Kroger–Vink (KV) notation) adjacent to an aluminum vacancy V'''_{Al} and the same assignment should also be true in LA_0. The observation of the optical absorption peaking at 3.1 eV reinforces this interpretation, as will be shown below. Since the magnetoplumbite structure has a variety of possible sites, an accurate determination of the O^- site requires a more detailed study of the ESR spectra.

Many of the characteristics of O^- type centers in oxides can be understood according to the simple model of Bartram, Swenberg, and Fournier (BSF) (*16*). In that model the cation vacancy creates an axial crystal field component acting on adjacent oxygen ions. This field leaves the threefold degeneracy of the O^{2-} $2p$ orbitals, the $2p_z$ level (z along the O^{2-} vacancy direction) being raised in energy (Fig. 7). The consequence is that an O^{2-} ion adjacent to a cation vacancy can trap a hole in its $2p_z$ orbital. According to the loss of divalent ions observed during the crystal growth (Table I), the cationic defect involved in defect A in LA_0 is V''_{Mg} rather than V'''_{Al}. The formation of the paramagnetic defect induced by X-ray excitation is summarized by

$$V''_{Mg} + O_0^x + h^\cdot \rightarrow (V''_{Mg} - O^\cdot)'. \quad (3)$$

A defect such as $(V''_{Mg} - O^\cdot)'$ is also known as a V^- center (*17*). From the simple crystal field theory of BSF, it is predicted that the g tensor should be axial, with two values:

$$g_\parallel = g_e$$

and

$$g_\perp = g_e - 2\lambda/\Delta \quad (4)$$

in which $g_e = 2.0023$ is the free-electron g value, $\lambda \simeq -135$ cm^{-1} (*17*) the spin-orbit coupling constant for a free O^{-1} ions, and Δ the splitting between the $2p_x$, $2p_y$, and $2p_z$ orbitals. According to the BSF model, Δ is given by (*17*)

$$\Delta = \frac{3|Z|}{5}\left(\frac{e^2}{R^3}\right)\langle r^2\rangle \quad (5)$$

where $\langle r^2\rangle = 3.04$ a.u. (*17*) is the mean value of the square of the electron–nucleus distance in a $2p$–O^- radial were function, $|Z| = 2$ the effective charge created by the cation vacancy, and R the anion–V_{Mg} separation. Since the model predicts the smallest g shift for B_0 along the $O^- - V_{Mg}$ direction, we can conclude that this is colinear to the [00.1] axis in LA_0. Only two cationic

sites with axial symmetry (C_{3v}) have an O^{2-} ion along the [00.1] axis:

(i) The Al(2) tetrahedral position (4*f* in Wyckoff notation) of the spinel blocks, with $R = 1.870$ Å and (ii) the Al(5) position (4*e* in Wyckoff notation) near the mirror plane, with $R = 1.996$ Å. These two R values lead, through expressions (4) and (5), to calculated perpendicular g shifts $\Delta g_\perp = g_\perp - g_e$ of 13.5×10^{-3} and 10×10^{-3}, respectively. The agreement with the experimental value $\Delta g_\perp = +14.7 \times 10^{-3}$ is good owing to the simplicity of the BSF model. Let us now consider the discrepancy between the experimental parallel g shift $\Delta g_\parallel = +6 \times 10^{-3}$ and the calculated one $\Delta g_\parallel \simeq 0$ (or $\Delta g_\parallel \simeq -\frac{1}{4}(\Delta g_\perp)^2 \simeq -10^{-4}$ including third-order correction in perturbation calculation (*17*)). A positive $\Delta g_\parallel$ can be accounted for by considering that the hole is not trapped at one O^{2-}, but that it is partially shared among all the O^{2-} ions adjacent to the cation vacancy (*18*). The O^{2-} ions should be approximately equivalent in order to allow the hole transference. This consideration favors the localization of the cation vacancy in tetrahedral Al(2) position of the spinel blocks.

The observation of an optical absorption band at 3.1 eV correlated to the defect A confirms its attribution to a $(V''_{Mg}\text{–}O^{\cdot})'$ center ($\equiv V^-$ center). Absorption bands near 3 eV exist also for the V-type centers in α-Al_2O_3 (*19*) and $MgAl_2O_4$ (*20*). These optical absorptions cannot arise from transitions between the *p* levels of the O^- ion split by the crystal field created by the cationic defect (see Fig. 7) because such transitions are forbidden ($\Delta l = 0$). Hence they cannot be responsible for the pronounced brown coloration of LA_0 crystals. More recently the absorption of V type centers was explained by a light-induced transfer of the hole from one equivalent O^{2-} site to another near the cation vacancy (*21*) according to

$$(O^x\text{–}V''_{Mg}\text{–}O^{\cdot})' \xrightarrow{h\nu} (O^{\cdot}\text{–}V''_{Mg}\text{–}O^x)'. \quad (7)$$

This mechanism, in its simplest form (*21*), predicts that the energy ΔE and the linewidth W of the optical absorption are related by

$$W \simeq 1/(2\Delta E \hbar\omega_0). \quad (8)$$

where $\hbar\omega_0$ is the phonon energy. By using the experimental values $\Delta E = 3.1$ eV and $W = 1.9$ eV for defect A, we found $\hbar\omega_0 \simeq 0.08$ eV, which is a typical value of $\hbar\omega_0$ in oxide materials.

(*b*). *Discussion of the other absorption bands.* Assignment of defect A was possible because it is represented both in ESR and OA spectra. After thermal bleaching of this defect the remaining weak absorption bands at 3.8, 2.8, and 2.1 eV, labeled B, C, and D (Fig. 4), are not associated to ESR signals. Consequently we shall propose only a tentative interpretation of these bands.

It should be noticed that the positions and widths of bands B and C are not markedly different from those of defect A. Their smallest width $W = 0.75$ eV (Fig. 4) results from the low temperature (15 K) used to record their optical spectrum. Increasing the temperature results in a significant increase of *W*. It is thus tempting to attribute the optical absorption bands B and C also to electron holes trapped at oxygen ions adjacent to cation vacancies, or cation impurities with charge lower than 3+. Defects A, B, and C probably correspond to a hole trapped by oxygen ions adjacent to different cationic defects. This is not unexpected since cationic defects are very likely to be distributed over several different sites of spinel blocks.

If we retain this interpretation of defects B and C, the absence of ESR signal for these defects needs some explanation. It should be noticed that the γ-ray-induced optical absorption at 3.1 eV in spinel $MgAl_2O_4$ has been assigned to O^- ions adjacent to cationic defects (*20*) although no corresponding ESR signal were detected.

Actually several possible features can be responsible for a considerable lowering of the ESR spectral intensity beyond the limit of detection. First of all a significant broadening of the signal may exist, due to unresolved *hf* interactions with ^{27}Al ($I = \frac{5}{2}$) nuclei of the structure. Most probably a low symmetry of the cationic site containing the defect would produce a site splitting of the ESR signal—i.e., a decomposition of the ESR signal into several components. This effect is for instance responsible for the poor signal to noise ratio of the ESR signal of V^{2-} centers in α-Al_2O_3 (*15*). If we assume similar oscillator strengths for the bands A, B, and C, the small concentration of defects B and C combined with ESR site splitting could be responsible for the apparent lack of ESR signals related to these defects.

An interpretation of the weak optical absorption band D, peaking at 2.1 eV, is more problematical since its width $W = 0.14$ eV at 15 K is too small to be consistent with a hole absorption.

IV.2. Radiation-Induced Valence Change of Fe^{3+} Impurities

Figure 8 shows the OA spectra in the region 220–290 nm of a single crystal of LA_0. They consist of a band centered at 4.8 eV flanking the fundamental absorption band. The former is more intense in crystals LA_0 doped with 0.5% Fe. Thermal treatments in air at 1200°C of these crystals further increase the intensity of the 4.8-eV band. These features indicate that this absorption band is due to a light-induced charge transfer between oxygen and Fe^{3+} ions according to

$$O^{2-}\text{–}Fe^{3+} \xrightarrow{h\nu} O^{-}\text{–}Fe^{2+} \qquad (9)$$

This interpretation of the 4.8-eV absorption band is confirmed by its similarity with the oxygen–Fe^{3+} transition in α-Al_2O_3 and $MgAl_2O_4$, which occurs at 4.7 and 4.8 eV, respectively (*22, 20*). The increase of the

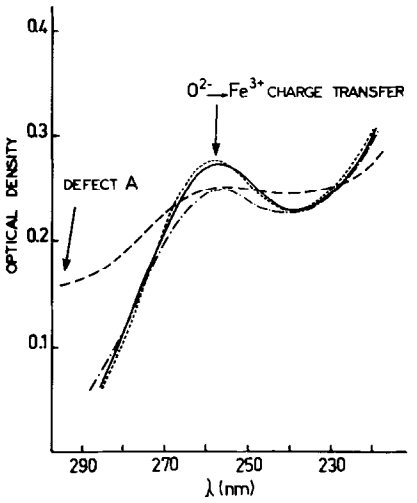

FIG. 8. Optical absorption spectra of LA_0 in the O^{2-}–Fe^{3+} charge-transfer region. (—) nonirradiated; (– – –) irradiated by X rays for 1 hr; (–·–·) 5 min at 140°C after irradiation; (···) 5 min at 380°C after irradiation.

4.8-eV band intensity after thermal treatments shows that iron impurities in LA_0 are present in both 2+ and 3+ oxidation states.

After X-ray irradiation of these crystals the 4.8-eV band is significantly reduced and superimposed to the tail of the hole absorption band A peaking at 3.1 eV (Fig. 8). A partial recovery of the 4.8-eV band is obtained by thermal treatment at 140°C during 5 min, which also produces the bleaching of the 3.1-eV band. A complete thermal bleaching of bands B and C restores the 4.8-eV absorption band at its initial intensity. This intensity change of the Fe^{3+} charge–transfer transition upon irradiation shows that a significant part of Fe^{3+} has been reduced into Fe^{2+}, and that the reverse reaction occurs during the thermal bleaching (TB) of bands A, B, and C

$$Fe^{3+} + e \underset{\text{TB}}{\overset{\text{X rays}}{\rightleftharpoons}} Fe^{2+} \qquad (10)$$

Charge transfer transitions of Fe^{2+} are not detected because the reduction in charge shifts these bands toward shorter

TABLE II

SUMMARY OF THE SPECTROSCOPIC RESULTS

Defect	Spectroscopy features	Assignment and localization	Concentration		Remark
			Before irradiation	After irradiation	
Mn^{2+}	ESR	Tetrahedral Al(2) sites of spinel blocks	Traces ~10 ppm	No change	Responsible for the green TSL
Fe^{3+}	ESR and optical absorption at 4.8 eV	Axially distorted Al(5) sites of mirror planes	Traces ~50–100 ppm	Decrease $Fe^{3+} + e \rightarrow Fe^{2+}$	
A	ESR and optical absorption at 3.1 eV	O^- ion adjacent to a cation vacancy in spinel blocks	Zero	Strong; responsible for the intense brown coloration of the crystals	Thermal bleaching at $T < 500$ K
B	Optical absorption at 3.8 eV	Probably O^- on adjacent to other cationic defects of spinel blocks	Zero	Weaker than defect A absorption	Thermal bleaching at $T > 500$ K detectable after bleaching of defect A
C	Optical absorption at 2.8 eV	"	Zero	"	
D	Optical absorption at 2.1 eV	Non identified	Zero	Very Weak	

wavelengths compared to the Fe^{3+} one. Hence they are hidden by the strong fundamental absorption of the matrix.

Further details about these Fe^{3+} impurities are obtained by ESR studies on as grown single crystals. For an orientation of the magnetic field B_0 parallel to the crystallographic axis [00.1], the ESR signal of Fe^{3+} consists of a single line at $g_{eff} \simeq 2.00$ (Fig. 5). The angular variation of this spectrum within 20° around the [00.1] direction is shown in Fig. 9. It is difficult to detect the ESR signal for B_0 orientation which are more than 10° apart from the [00.1] direction because the shift toward low field of the signal is accompanied by a considerable broadening of the line. The experimental variation of g_{eff} shows that the site occupied by Fe^{3+} experiences a strong axial distortion along the [00.1] direction. In that case the two components of g_{eff} are given by (*23*)

$$g_{\parallel eff} = g_{\parallel}$$

and

$$g_{\perp eff} = 3g_{\perp}\left[1 - \frac{2(g_{\perp}\beta M)^2}{(2D)^2}\right] \qquad (11)$$

with D being the axial zero-field splitting parameter. Since g is almost isotropic ($g_{\parallel} = g_{\perp}$) and very close to 2.00 for a $^6S_{5/2}$ ion and assuming $D \gg g\beta H$, we would expect $g_{\parallel} = 2.0$ and $g_{\perp eff} = 6.0$. Under this assumption, the angular variation $g_{eff}(\theta)$ can be written for small values of θ (*23*)

$$g_{eff}(\theta) = g(1 + 8 \sin^2 \theta)^{1/2}. \qquad (12)$$

Figure 9 compares the experimental g_{eff} values and those calculated using expression (*12*). The good agreement confirms

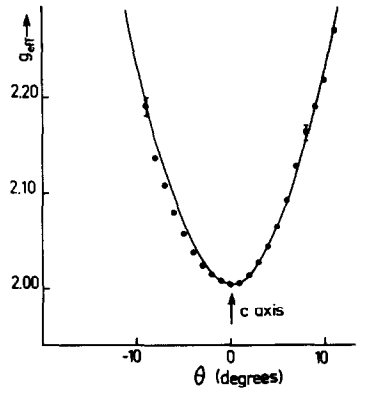

FIG. 9. ESR of Fe^{3+} in LA_0. Variation of g_{eff} with the orientation of the magnetic field B_0 with respect to the crystallographic axis c ([00.1] direction). Full line: calculated.

that we are in the strong axial field case ($D \gg g\beta H$).

It should be emphasized that only the site Al(5) of the mirror planes (Fig. 1) experiences a sufficiently strong axial distortion to be consistent with the Fe^{3+} ESR features. This site can be described as a trigonal bipyramid (symmetry D_3h) elongated along the C_3 axis. However, the cation is not located in the equatorial plane of the polyhedron, but is shifted from the plane along the C_3 axis. Hence this site should be rather described as an axially distorted tetrahedral site with C_{3v} symmetry. X-Ray diffraction studies (*3*) have shown that Al^{3+} in this site has the oxygen O(1) at 1.763 Å and one oxygen O(4) at 1.996 Å, the other oxygen O(4) being at 2.491 Å. It is known that in rare earth hexaferrites with magnetoplumbite structure (*24*) Fe^{3+} in this site experiences the same shift from the mirror plane, reducing the coordination polyhedron of Fe^{3+} to a distorted tetrahedron.

IV.3. Stability of Mn^{2+} Impurities

It has been noticed that the transition $^4T_1 \rightarrow {}^6A_1$ of Mn^{2+} ions is responsible for the green TSL observed in LA_y compounds. It is thus important to investigate the stability of manganese charge state under irradiation and thermal recombination. Figure 10 shows the $M_I = \frac{5}{2}$ h.f. line of the $M_S = \frac{1}{2} \leftrightarrow -\frac{1}{2}$ transition of Mn^{2+} in $LA_{0.01}$, recorded before and after exposure to X rays during 1 hr. Irradiation induces no change of the ESR intensity, the small difference being due to a misorientation of the crystal in the magnetic field. Manganese is thus radiation stable, because a valence change of Mn^{2+} upon irradiation would lead to Mn^{3+} ($3d^4$) and this ion gives no ESR at room temperature. The net result would be a decrease of the ESR intensity of Mn^{2+}, which is not observed in our experiments. The same behavior is found for $y > 0.01$, and also for $y = 0$ (Fig. 5).

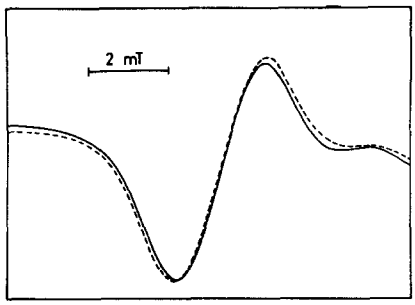

FIG. 10. $M_I = \frac{5}{2}$ hyperfine line of the $M_s = \frac{1}{2} \rightarrow -\frac{1}{2}$ transition of Mn^{2+} in $La_{0.01}$. Full line: before irradiation. Dotted line: after 1 hr irradiation by X rays. B_0 is parallel to the [00.1] axis.

V. Discussion

When a crystal is irradiated by X rays, electrons and holes are formed in the conduction and valence bands, respectively. Electrons and holes can then be trapped at defects or impurities if the temperature is low enough. In the case of LA_y compounds, electrons are trapped at Fe^{3+} impurities and holes at oxygen ions adjacent to charge deficient cationic sites. These defects are identified by their OA and, for two of them, by their ESR spectra. The following equations summarize the effect of X ray irradiation:

$$\text{X rays} \rightarrow e' + h^{\cdot}$$

$$e' + Fe^{3+} \rightarrow Fe^{2+}$$

$$h^{\cdot} + O_0^x + V''_{Mg} \rightarrow (O^{\cdot} - V''_{Mg})'(\equiv \text{defect A}) \quad (13)$$

Hole trapping at other cationic defects leads to the formation of defects B and C.

Thermal recombination of these defects is responsible for the observed TSL. A TSL peak is due to the recombination of a charge, which is thermally released from a trap, with the opposite charge which is more strongly trapped. Let us first consider the TSL peak at low temperature (~95°C). It is associated with the complete bleaching of defect A and with a partial recovery of the OA and ESR spectra of Fe^{3+}. This be-

havior indicates that holes are thermally released in the valence band from defect A, and recombine with Fe^{2+} to give Fe^{3+} in an excited state $(Fe^{3+})^*$ according to

$$(O_O^{\cdot}\text{–}V''_{Mg})' \rightarrow O_O^{x}\text{–}V''_{Mg} + h^{\cdot}$$
$$h^{\cdot} + Fe^{2+} \rightarrow (Fe^{3+})^*. \qquad (14)$$

If the other possibility holds—i.e., the thermal release of the electrons from Fe^{2+}—we should expect a complete restoration of Fe^{3+} spectra and a partial decrease of the intensity of the three hole centers A, B, and C simultaneously, in contradiction with our observations. Since the holes migrate in the valence band formed by oxygen orbitals, the iron-excited state which forms when O^- reaches the vicinity of a Fe^{3+} ion probably corresponds to the charge-transfer state (O^-–Fe^{3+}). This state is also formed when Fe^{3+} in its ground state absorbs a 4.8-eV photon (see reaction (*9*)). Partial deactivation of $(Fe^{3+})^*$ via radiationless multiphonon processes leads to Fe^{3+} excited into the $^4T_1$ level. The $^4T_1 \rightarrow {}^6A_1$ transition of Fe^{3+} in cubic symmetry is rather frequently observed in luminescence spectra of minerals (*26*). For example, it occurs at 15,255 cm^{-1} (~660 nm) for Fe^{3+} in tetrahedral sites of $LiAl_5O_8$ spinel. It is then obvious that the transition does not contribute to the green TSL in LA_y, occurring at 19,230 cm^{-1} (520 nm) and which was attributed to the $^4T_1 \rightarrow {}^6A_1$ transition of Mn^{2+} in tetrahedral sites of LA_y spinel blocks. Since manganese retains its 2+ oxydation state during both irradiation and thermal recombination processes, the Mn^{2+} emission is most probably due to a transfer of excitation from Fe^{3+} to Mn^{2+} according to

$$[Fe^{3+}(^4T_1)]^* + Mn^{2+}(^6A_1) \rightarrow Fe^{3+}(^6A_1) + [Mn^{2+}(^4T_1)]^*$$
$$[Mn^{2+}(^4T_1)]^* \rightarrow Mn^{2+}(^6A_1) + h\nu\ (520\ nm) \qquad (15)$$

From this point of view, the TSL of LA_y can be considered as a sensitized TSL, with Mn^{2+} acting as ion activator. Nevertheless it should be noticed that there is probably a large energy mismatch ΔE_{sa} of approximately 4000 cm^{-1} between the Fe^{3+} and Mn^{2+} transitions. Since ΔE_{sa} is several times the highest phonon energy of oxide materials, the energy transfer should take place via a multiphonon process (*27*). In this case a transfer between ions without electronic energy overlap is possible provided that the overall energy conservation is maintained by the simultaneous annihilation of several phonons. However, the energy mismatch ΔE_{sa} could be smaller than 4000 cm^{-1} since ESR has shown that Fe^{3+} occupies a strongly distorted tetrahedral site of C_{3v} symmetry. Its $^4T_1$ state is thus split by the axial crystal field into $^4A_2$ and ^4E states. One of these two states, raised in energy with respect to the $^4T_1$ state, could then approach the energy of the $^4T_1$ Mn^{2+} state.

The mechanism for the two TSL peaks at 210 and 320°C is probably similar to that of the peak at 95°C since it involves the same electron trap Fe^{3+} and the same Mn^{2+} activator ion. The hole traps are now B and C centers and the higher temperatures of the TSL result from higher binding energies (1.0 and 1.2 eV instead of 0.7 eV) of the holes in B and C centers.

The variation of the green TSL intensity with respect to the temperature of the glow peaks in LA_0 (Fig. 3) can be qualitatively explained according to the multiphonon assisted energy transfer discussed above. Although center A is the most important hole trap, its thermal recombination at 97°C leads only to a very weak green TSL while recombination of defects B and C at higher temperature—at which more phonons are available to assist the energy transfer—lead to a strong green TSL. If N is the number of phonons involved in the process, the energy transfer rate rises steeply with temperature as $W \propto [kT/\hbar\omega]^N$ (*27*). For a given concentration of hole centers, the intensity of

the manganese emission should thus increase as $I \propto T^N$.

The increase of manganese concentration y in LA_y results in two effects: (i) From $y = 0$ to $y = 0.01$ there is a strong increase of the peak intensities at all temperatures. This effect is particularly important at low temperature; (ii) for $y \geq 0.07$ there is a concentration quenching of the TSL. This effect increases with temperature so that the TSL intensity at low temperature is only slightly affected by the increase of y while the TSL peaks at 210 and 320°C strongly decrease with increasing y and vanish, respectively, for $y \geq 0.27$ and $y \geq 0.15$. These last features can be explained by an increase of the efficiency of the concentration quenching process with increasing temperatures. At high manganese concentration, energy migration between Mn^{2+} ions can occur. Because of the efficiency of this energy transfer between identical ions (*27*), the excitation may ultimately reach a quenching trap, and dissipate thermally (*27*). A previous ESR study of Mn^{2+} in LA_y compounds (*10*) has shown that these ions experience crystal field disorder and (or) statistical distribution among different sites. Thus some Mn^{2+} with their $^4T_1$ levels lying at lower energy than the other Mn^{2+} ions can act as luminescent traps. Under these conditions, the evolution with temperature of the intensity of the green TSL in LA_y ($y > 0.07$) can be tentatively explained in the following way.

(i) Near room temperature, Fe^{3+} [$^4T_1$] transfers its excitation to a neighboring Mn^{2+} [$^4T_1$] trap from which the green luminescence occurs.

(ii) At higher temperatures, $^4T_1$ states of regular Mn^{2+} ions are thermally populated at the expense of the Mn^{2+} [$^4T_1$] traps. The excitation is again transferred along chains of Mn^{2+} ions until it comes into the vicinity of a quenching trap. Consequently the higher the temperature the lower is the population of the luminescent traps and the higher is the concentration quenching efficiency.

References

1. D. Gourier, D. Vivien, and J. Livage, *Phys. Status Solidi A* **56,** 247 (1979); K. O'Donnell, R. C. Barklie, and B. Henderson, *J. Phys. C* **11,** 3871 (1978).
2. A. Kahn, A. M. Lejus, M. Madsac, J. Thery, D. Vivien, and J. C. Bernier, *J. Appl. Phys.* **52,** 6864 (1981).
3. M. Gasperin, M. C. Saine, A. Kahn, F. Laville, and A. M. Jejus, *J. Solid State Chem.* **54,** 61 (1984).
4. A. L. N. Stevels, *J. Lumin.* **20,** 99 (1979), and references therein; M. Tamatani, *Jpn. J. Appl. Phys.* **13,** 950 (1974).
5. D. Vivien, A. M. Lejus, J. Thery, R. Collongues, J. J. Aubert, R. Moncorge, and F. Auzel, *C.R. Acad. Sci. Ser. II* **298,** 195 (1984).
6. V. M. Garmash, A. A. Kaminskii, M. J. Polyakov, S. E. Sarkisov, and A. A. Filimonov, *Phys. Status Solidi A* **75,** K111 (1983).
7. M. Tamatani, *Jpn. J. Appl. Phys.* **13,** 957 (1974).
8. O. F. Schirmer, K. W. Blazey, W. Berlinger, and R. Diehl, *Phys. Rev. B* **11,** 4201 (1975).
9. F. Laville and A. M. Lejus, *J. Cryst. Growth* **63,** 426 (1983).
10. F. Laville, D. Gourier, A. M. Lejus, and D. Vivien, *J. Solid State Chem.* **49,** 180 (1983).
11. Microprobe analyses were performed at the "Centre d'analyse par microsonde Comparis." Laboratoire de Petrologie, Université Pierre et Marie Curie, Paris, France.
12. F. Urbach, *Winer. Ber. IIA,* 139 (1930).
13. W. Hoogenstraaten, *Philips Res. Rep.* **13,** 515 (1958).
14. V. A. Lebedev, V. F. Pisarenko, and V. V. Popov, *Izv. Akad. Nauk SSSR, Neorg. Mater.* **19,** 1356 (1983).
15. K. H. Lee, G. E. Holmberg, and J. H. Crawford, *Solid State Commun.* **20,** 183 (1976), and reference therein.
16. R. H. Bartram, C. E. Swenberg, and J. T. Fournier, *Phys. Rev.* **139,** 941 (1965).
17. A. E. Hughes and B. Henderson, *in* "Point Defects in Solids," (J. H. Crawford and L. M. Slifkin, Ed.), Vol. 1, Plenum, New York (1972).
18. T. C. Ensign and S. E. Stokowski, *Phys. Rev. B* **1,** 2799 (1970).
19. K. H. Lee, G. E. Holmberg, and J. H. Crawford, *Phys. Status Solidi A* **39,** 669 (1977).

20. G. S. WHITE, R. V. JONES, AND J. H. CRAWFORD, *J. Appl. Phys.* **53,** 265 (1982).
21. O. F. SCHIRMER, P. KOIDL, AND H. G. REIK, *Phys. Status Solidi B* **62,** 385 (1974); O. F. SCHIRMER, *J. Phys. Colloque C6* **41,** 479 (1980).
22. H. H. TIPPINS, *Phys. Rev. B* **1,** 126 (1970).
23. E. S. KIRKPATRICK, K. A. MULLER, AND R. S. RUBINS, *Phys. Rev. A* **135,** 86 (1964).
24. X. OBRADORS, J. TEJADA, A. ISALGUE, AND J. C. JOUBERT, *Solid State Commun.* **50,** 821 (1984), and references therein.
25. A. LORINCZ, M. PUMA, F. J. JAMES, AND J. H. CRAWFORD, *J. Appl. Phys.* **53,** 927 (1982).
26. D. T. PALUMBO, *J. Lumin.* **4,** 89 (1971).
27. T. MIYAKAWA AND D. L. DEXTER, *Phys. Rev. B* **1,** 2961 (1970); R. C. POWELL AND G. BLASSE "Structure and Bonding," Vol. 42, p. 43, Springer-Verlag, New York/Berlin (1980).